Research Article | Vol. 27, No. 3 | 4 Feb 2019 | OPTICS EXPRESS 2212
Optics EXPRESS

# Interaction-free ghost-imaging of structured objects

YINGWEN ZHANG,[1] ALICIA SIT,[1] FRÉDÉRIC BOUCHARD,[1] HUGO LAROCQUE,[1] FLORENCE GRENAPIN,[1] ELIAHU COHEN,[1,2] AVSHALOM C. ELITZUR,[3,4] JAMES L. HARDEN,[1] ROBERT W. BOYD,[1,5] AND EBRAHIM KARIMI[1,*]

[1]*Physics Department, Centre for Research in Photonics, University of Ottawa, Advanced Research Complex, 25 Templeton, Ottawa, ON K1N, 6N5 Canada*
[2]*Faculty of Engineering and Institute of Nanotechnology and Advanced Materials, Bar Ilan University, Ramat Gan 5290002, Israel*
[3]*Iyar, The Israeli Institute for Advanced Research, POB 651, Zichron, Ya'akov 3095303, Israel*
[4]*Institute for Quantum Studies, Chapman University, Orange, CA 92866, USA*
[5]*Institute of Optics, University of Rochester, Rochester, New York 14627, USA*
[*]*ekarimi@uottawa.ca*

**Abstract:** Quantum – or classically correlated – light can be employed in various ways to improve resolution and measurement sensitivity. In an "interaction-free" measurement, a single photon can be used to reveal the presence of an object placed within one arm of an interferometer without being absorbed by it. With a technique known as "ghost-imaging", entangled photon pairs are used for detecting an opaque object with significantly improved signal-to-noise ratio while preventing over-illumination. Here, we integrate these two methods to obtain a new imaging technique which we term "interaction-free ghost-imaging" (IFGI). With this new technique, we reduce photon illumination on the object by up to 26.5% while still maintaining at least the same image quality of conventional ghost-imaging. Alternatively, IFGI can improve image signal-to-noise ratio by 18% when given the same number of interacting photons as in standard ghost-imaging. IFGI is also sensitive to phase and polarisation changes of the photons introduced by a structured object. These advantages make IFGI superior for probing light-sensitive materials and biological tissues.



## 1. Introduction

Quantum metrology enables single photons, entangled photon pairs, or multi-photon quantum states to be used for enhancing the resolution of measurements [1]. Such states are now applied in several imaging schemes such as interaction-free imaging [2], ghost-imaging [3, 4], imaging using N00N-states [5] and sub-shot-noise imaging [6, 7]. Interaction-free imaging involves a single photon going through an interferometer and revealing an object's presence or of its physical properties by the *absence* of a visible interaction with it [2]. If undisturbed in the interferometer, the photon interferes with itself and exits through only one output port, leaving the other port "dark". If, however, an object is placed in one arm of the interferometer, then the photon's interference is disturbed and the detection of photons in the supposedly dark output port of the interferometer will occur. The key aspect of this technique relies on the fact that photons detected in the dark output port have never interacted with the object, yet can still reveal its presence. Enhancements of the original method [8] involve the quantum Zeno effect [9, 10], as well as more elaborate schemes based on induced coherence without induced emission [11]. Similar interaction-free measurements have also found many applications in quantum computation and communication [12, 13], stabilizing ultracold atoms [14], orbital angular momentum spectrometry [15] and optical switching [16].

#352797 https://doi.org/10.1364/OE.27.002212
Journal © 2019 Received 26 Nov 2018; revised 23 Dec 2018; accepted 23 Dec 2018; published 24 Jan 2019

Optics EXPRESS

Entangled photon pairs produced through spontaneous parametric down-conversion (SPDC) can be used to produce images with high signal-to-noise ratio (SNR). In ghost-imaging [17–20], one of the down-converted photons is used to illuminate an object and is captured by a bucket detector. The other is sent through a different path to a camera. By registering only coincidence events between the camera and the bucket detector, an image of the object is formed on the camera even though the photons collected by the camera have never interacted with the object. This significantly reduces the background noise in the obtained images, giving them a high SNR and allowing images to be obtained with an average of fewer than one detected photon per image pixel [21]. Ghost imaging schemes, relying on non-degenerate down-converted photon pairs, have also been demonstrated [22]. Ghost imaging can also be achieved with classical light [23–28]; however, using classical light does not seem to have all the above mentioned perks of using entangled photons. A comprehensive study of the SNR from classical and quantum ghost imaging can be found in [29, 30]. A major disadvantage of ghost-imaging is its inability to directly image birefringent and phase-only objects [23].

Here, we merge the two ideas and demonstrate interaction-free ghost-imaging (IFGI) which possesses the benefits of both techniques. In IFGI, an interferometer is built along the path of the photon used to probe the object; a bucket detector is placed at each of the exit ports. If no object is present, then photons will only be registered in the exit port with constructive interference. However, once an object is placed in one arm of the interferometer, the interference is disturbed and both bucket detectors may detect photons. By subtracting the image obtained in the destructive interference port from that of the constructive port, we can obtain an image with comparable SNR compared to that of conventional ghost-imaging (CGI) while reducing photon illumination on the object by up to 26.5%. If we were to allow the same number of photons to illuminate the object, then IFGI would be able to improve SNR by a factor of 18% compared to CGI. This feature could be of great importance in imaging objects that display high sensitivity to light, such as photoreceptor cells. Furthermore, we show that IFGI is also very sensitive to both phase and polarisation changes in the beam and can be used to image birefringent and phase-only objects.

## 2. Theoretical SNR of IFGI

In order to compare the performance of IFGI with CGI, we employ the commonly used figure of merit, the SNR, given by, [31]

$$\mathrm{SNR} = \frac{1}{\sigma}|\bar{I}_{\mathrm{in}} - \bar{I}_{\mathrm{out}}|, \tag{1}$$

where $\bar{I}_{\mathrm{in}}$ and $\bar{I}_{\mathrm{out}}$ are the average intensity values of the reconstructed ghost-image, inside and outside the object profile, respectively, and $\sigma := \sigma(\bar{I}_{\mathrm{in}} - \bar{I}_{\mathrm{out}})$ is the standard deviation in the intensity difference.

Ideally, for CGI, when an average of $\bar{N}$ photons is used to interrogate an object in the time interval $t_{\mathrm{int}}$, all $\bar{N}$ photons will be absorbed/scattered by the object, giving a change in photon number (signal strength) at the detector of $\Delta N_{\mathrm{CGI}} = -\bar{N}$. As SPDC has Poissonian statistics in the coincidence count rate, the SNR is then,

$$\mathrm{SNR}_{\mathrm{CGI}} = \frac{\bar{N}}{\sqrt{\bar{N}}} = \sqrt{\bar{N}}. \tag{2}$$

Now, for IFGI, let us assume, for simplicity, a Mach-Zehnder interferometer with the input beam splitter (BS) having reflectivity $R$ and transmissivity $T$, and the exit BS having reflectivity $T$ and transmissivity $R$ (See the Appendix for more details). If an average of $\bar{N}$ photons enters the first BS during the same time interval $t_{\mathrm{int}}$, and the object is placed in the transmission arm of the interferometer, then in the constructive exit port, a change in photon number of $\Delta N_C = \bar{N}(R^2 - 1)$

will be observed. In the destructive exit port, a change of $\Delta N_D = \bar{N}RT = \bar{N}R(1-R)$ will be observed. Subtracting $\Delta N_D$ from $\Delta N_C$ gives,

$$\Delta N_{\mathrm{IFGI}} = \bar{N}(2R^2 - R - 1). \tag{3}$$

Therefore, to have $\Delta N_{\mathrm{IFGI}} = \Delta N_{\mathrm{CGI}}$ will require $R = T = 0.5$ (ignoring the trivial case of $R = 0$). This means that only $\bar{N}/2$ photons will have interacted with the object, effectively reducing the interaction by half compared to CGI, while maintaining the same signal strength. Moreover, when $R < T$, one can obtain $\Delta N_{\mathrm{IFGI}} > \Delta N_{\mathrm{CGI}}$ with a maximum of 12.5% increase in signal strength when $R = 0.25$ ($T = 0.75$). From this, the SNR of IFGI is determined to be,

$$\mathrm{SNR}_{\mathrm{IFGI}} = \frac{\left|2R^2 - R - 1\right|}{\sqrt{1+R}}\mathrm{SNR}_{\mathrm{CGI}}, \quad \text{for equal } t_{\mathrm{int}}\ . \tag{4}$$

Here we observe that, within the same interrogation time $t_{\mathrm{int}}$, even though the signals from the two output ports of the interferometer is subtracted from each other, which resulted an increase in the noise by a factor of $\sqrt{1+R}$. However, the overall signal strength changes according to $\left|2R^2 - R - 1\right|$, which increases faster than the noise for $R < 0.265$ giving IFGI a slightly better image SNR when compared to CGI for $R < 0.265$. This improvement holds a maximum value of 3.1% when $R = 0.124$. This indicates that it is possible to reduce photon interaction with the object by a maximum of 26.5% compared to CGI without any reduction in the image quality.

Now, if one were to allow the same number of photons to interact with the object in IFGI as in CGI (equal $N_{\mathrm{int}}$), an average total photon number of $\bar{N}/(1-R)$ will be required to enter the IFGI interferometer. This will then give a SNR of,

$$\mathrm{SNR}_{\mathrm{IFGI}} = \frac{\left|2R^2 - R - 1\right|}{\sqrt{1-R^2}}\mathrm{SNR}_{\mathrm{CGI}}, \quad \text{for equal } N_{\mathrm{int}}\ . \tag{5}$$

Here, due an increased number of photons entering the interferometer, the overall noise is actually lesser than in CGI by a factor of $\sqrt{1-R^2}$. This results in an even better SNR, with the maximum $\mathrm{SNR}_{\mathrm{IFGI}}$ obtained at $R = 0.366$, giving an 18% SNR improvement over CGI.

When analyzing the image quality, we used only the SNR as a figure of merit instead of the other commonly used quantity, the visibility, defined as $V = |\bar{N}_{\mathrm{in}} - \bar{N}_{\mathrm{out}}|/(\bar{N}_{\mathrm{in}} + \bar{N}_{\mathrm{out}})$ to compare the two methods. As making a fair comparison between IFGI and CGI would require a direct comparison between the number of photons used to create the image. However, $V$ is a normalized quantity and can give the same value provided that its ratio is maintained irrespective of the number of photons. Also $\bar{N}_{\mathrm{in}}$ will become negative for $R < 0.5$, giving $V > 1$ which is not a sensible value. Therefore, $V$ is not a suitable figure of merit to compare the two methods.

## 3. Experimental setup

As shown in the schematics in Fig. 1, a 0.5-mm-thick Type-I BiBO crystal is pumped by a 100 mW, 355 nm beam (Lumentum Xcyte CY-SM100) to generate position and momentum entangled photon pairs via SPDC. The 355 nm pump beam is afterwards filtered out with a long-pass filter. The photon pairs are probabilistically separated by a 50:50 BS where one photon is sent into an interferometer to probe an object and the other to an ICCD camera (Andor iStar CCD 334) where the image of the probed object is to be viewed. A Sagnac interferometer is constructed to ensure better stability of the interference. The clockwise and anti-clockwise beam paths of the interferometer are slightly displaced from each other such that the object can be placed in just one of the paths. A VBS – composed of a HWP and a PBS – was used to construct the interferometer in order to give us control over the amount of photons sent to probe the object. Imaging lenses are used to ensure that the ICCD camera and the object are

Optics EXPRESS

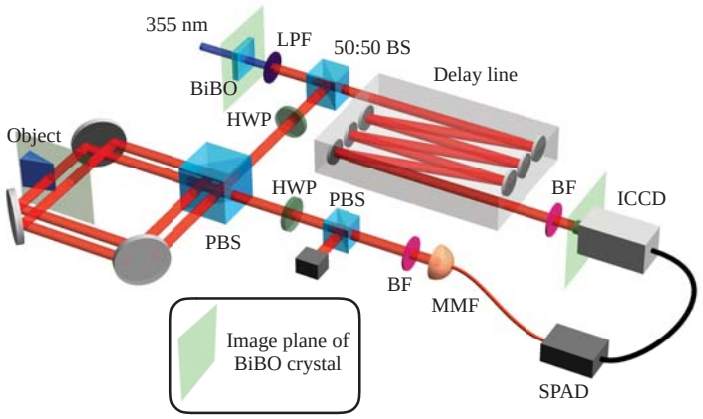


Fig. 1. Simplified schematic of the experimental setup for IFGI. Entangled photon pairs are generated at a nonlinear crystal (BiBO). One photon is sent into an interferometer with the object to be interrogated; the second photon is sent to a camera through a image preserving delay line where the image of the object is formed. Imaging lenses are not shown in the schematic. Figure legends: BiBO - 0.5 mm thick bismuth triborate crystal; LPF - Long-Pass Filter; BS - Beam Splitter; HWP - Half-wave plate; PBS - polarizing beam splitter; BF - Bandpass Filter; MMF - Multi-Mode Fibre; SPAD - Single Photon Avalanche Diode; ICCD - Intensified CCD camera.

in the same image-plane of the BiBO crystal. A second VBS is placed in the exit port of the interferometer allowing us to observe either constructive or destructive interferences. A bucket detector composed of a multi-mode fibre with a core diameter of 200 $\mu$m connected to a single photon avalanche diode (SPAD) (Excelitas SPCM-AQRH-14-FC) is placed behind this second VBS. The ICCD camera is triggered by the SPAD to detect coincidence events between the two arms (details on the specifications of the laser, SPAD and camera can be found in the Appendix). To compensate for the timing delay caused by the electronics, an image-preserving delay line [19] of 24 meters is placed in the path of the photons incident on the ICCD camera. The gating time on the ICCD is set to 5 ns. Bandpass filters of $710 \pm 5$ nm are placed in front of the ICCD and bucket detector so that only degenerate photon pairs are detected. Our IFGI setup can be converted into a CGI setup by simply adjusting the VBS to be fully transmissive. Using this setup, we were able to achieve a count rate of approximately $6 \times 10^5$ photons per second at the bucket detector, which allowed for the maximum triggering rate on our ICCD camera. Through this setup, we were able to achieve almost real time quantum ghost-imaging which makes searching for the image plane of the object on the ICCD much easier. This can be seen in Fig. 2, where the video of an “UO" sign moved into the beam path, taken with both VBS set to transmissive only, is displayed frame by frame. The integration time for each frame is only 1 second.

When making coincidence measurements, one also has to consider the subtraction of accidental events caused by background light, detector noise, etc. To account for accidental events during measurements, we adjust the delay of our ICCD such that, when triggered by the bucket detector, it opens its shutter just outside the coincidence window thereby registering only accidental events. The image obtained this way is subtracted off as background (more details on background subtraction can be found in the Appendix).

The final IFGI image is obtained by first taking an image with the second VBS set to constructive interference and then another image with the VBS set to destructive interference. The two images are then subtracted from each other, as shown in Fig. 3, to obtain the final IFGI image. It is important to note that, ideally, one would like to place a bucket detector at each of the constructive

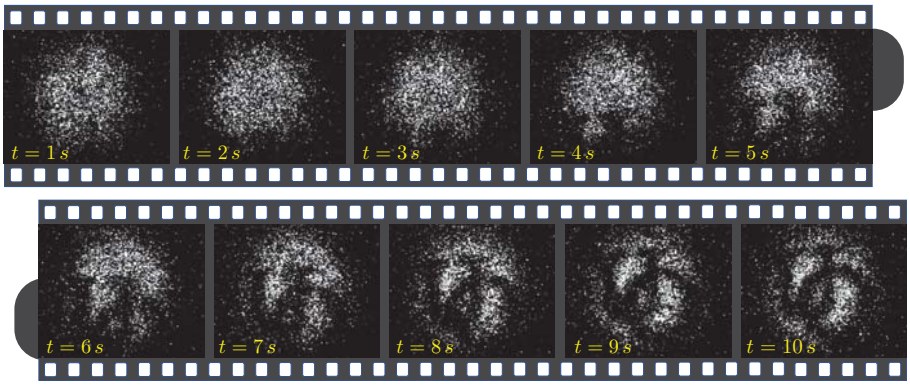


Fig. 2. Video frames taken with CGI (VBS adjusted to have $R = 0$) of an "UO" sign moved into the beam path. The integration time for each frame is 1 second.

and destructive output ports of the second VBS and have them trigger the same camera in parallel so two images, one for each output port, can be acquired at the same time. However, such a camera is not currently available to us, so we have opted for the current setup as a proof of principle.

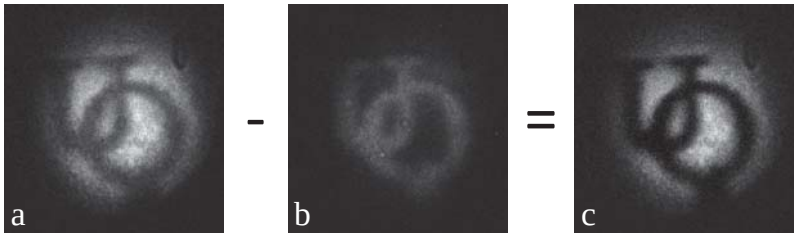


Fig. 3. Generation of an IFGI image. The final IFGI image (c) is obtained by subtracting the image of destructive interference (b) from constructive interference (a). Here, the VBS is set to 50:50 and the integration time is 150 s.

## 4. Experimental results

In order to verify Eqs. (4) and (5), we took images of a ~2 mm diameter laser cut metal sign of the letters "UO", Fig. 4(a), within a certain range of VBS R:T ratios. An image of the "UO" sign is first taken using CGI by setting the VBS to transmission only, Fig. 4(b); its SNR is then determined using Eq. (1) and used as the reference. First, to verify Eq. (4), we took images of the object at a range of VBS ratios with the same $t_{\text{int}} = 150$ s as in CGI. Their corresponding SNR is then determined and compared to the reference SNR from the CGI image. This is plotted in Fig. 5 as the blue squares with the corresponding theoretical prediction given by Eq. (4) plotted as the blue line. Now, to verify Eq. (5), we need to allow the same amount of photons $N_{\text{int}}$ to interact with the object as in CGI; this is done by increasing $t_{\text{int}}$ by a factor of $1/(1 - R)$. The experimental result of SNR for equal $N_{\text{int}}$ is plotted in Fig. 5 as the orange circles with the corresponding theoretical prediction given by Eq. (5) plotted as the orange line.

From these results, we can verify that by using IFGI, it is indeed possible to reduce photon illumination on the sample, without any loss in the image quality, up to a maximum of 26.5% when compared to CGI. Moreover, if one were to allow the same amount of illumination on the sample as in CGI, then IFGI is capable of improving SNR in the image up to 18%. The

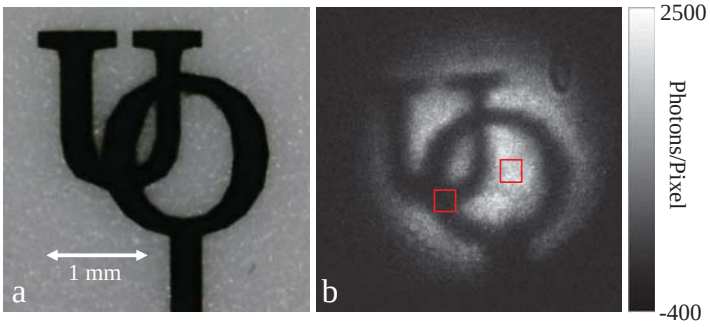


Fig. 4. Image of a metallic “UO" sign taken with CGI. (a) shows the imaged laser cut metallic sign of the letters “UO", with ~2 mm diameter. (b) shows its image taken using CGI with $t_{\text{int}}$ = 150 s. By recording the average photons/pixel and corresponding standard deviation in the regions enclosed by the red squares then using Eq. (1), the SNR of the image is calculated to be 7.28.

discrepancies between the experimental data and the theoretical calculations is mainly attributed to imperfections in the PBSs and HWPs.

Another advantage of IFGI when compared to CGI, thanks to the built-in interferometer, is in its sensitivity to changes in phase and polarisation of the photons. To demonstrate phase sensitivity, a ~0.15-mm-thick glass shard, Fig. 6(a), is placed in the beam and imaged by CGI, Fig. 6(b), and IFGI, Fig. 6(c). Using CGI, we can see that the area blocked by the glass shard is dimmer. This would be caused by the back reflection and scattering of photons in the glass. If the glass shard is anti-reflection treated, then it should be almost totally invisible to CGI except for perhaps the edges. With IFGI, the phase shift introduced by the glass disturbs the interference making the glass shard clearly visible.

The sensitivity to polarisation of IFGI is also demonstrated in Fig. 6. Here, a pattern of a “bomb" is imprinted on a liquid crystal device [32]; an image of the device placed between two cross polarisers is shown in Fig. 6(d). Any linearly polarised photons passing through the pattern will have their polarisation rotated by 90°. For a CGI setup, there are normally no polarisation sensitive elements so, both VBSs were removed from the setup when the CGI image was taken. The CGI image taken without any VBS is shown in Fig. 6(e) and this polarisation change is clearly not observed. However, the bomb pattern is clearly visible in Fig. 6(f) when IFGI is used, indicating a sensitivity to polarisation change. Polarisation sensitivity can certainly be added to CGI simply by placing a polariser after the object, but what we want to demonstrate here is that polarisation sensitivity is an intrinsic feature to IFGI. To compensate for the phase change introduced by the liquid crystal device, a glass plate of similar thickness is inserted in the other interferometer arm and with its insertion angle adjusted such that a good interference (> 70% visibility) is observed by the bucket detector.

On the fundamental side, our demonstration proves once again the robustness of quantum nonlocality and interaction-free measurement, even when combined together. Although ghost-imaging could similarly work for classically correlated light (with a predetermined direction of the photons) [23–25], we have used here nonlocally correlated photons (with the aim of further utilizing in the future the quantum features of the photons, e.g. when employing N00N or squeezed states). We have, therefore, found evidence that interaction-free measurements performed with the aid of one photon leads to “collapse", thereby affecting its remote entangled partner. The nonlocal features are clearly apparent in previous proposals along these lines [33–36], but in this experiment we chose to focus on the interaction-free aspects. The introduction of interaction-free imaging makes the present experiment genuinely quantum [37]. Moreover, it is

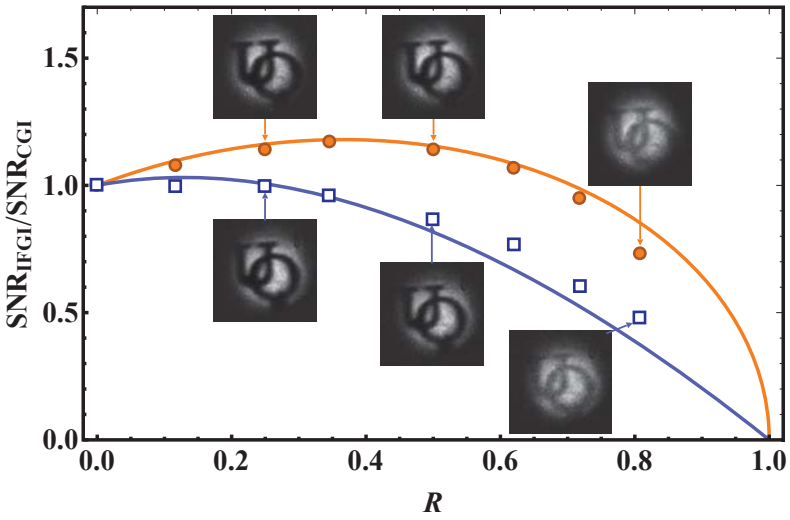


Fig. 5. Ratio between the SNR obtained using IFGI and that of CGI as a function of the VBS reflectivity $R$. The □ are the experimental data for when $t_{\text{int}}$ remains the same between IFGI and CGI, and the blue line is the corresponding theoretical prediction given by Eq. (4). The • are the experimental data for when $N_{\text{int}}$ remains the same between IFGI and CGI; this is achieved by increasing $t_{\text{int}}$ of IFGI by a factor of $1/(1-R)$. The orange line is the corresponding theoretical prediction given by Eq. (5). The insets are images taken with IFGI to determine the SNR at the indicated data points. The SNRs are determined from the same regions in the images as that indicated in Fig. 4(b). See the Appendix for the corresponding images of all the data points.

"doubly-nonlocal" since it employs both the familiar quantum nonlocality made possible through entanglement, as well as the more subtle nonlocality of two wavepackets corresponding to the same particle [38]. Notice that the latter enables one to sense not only the presence of an object, but also its properties, without necessarily changing it (by virtue of a quantum counterfactual interaction). Eventually, the unwanted effect of the photon on the probed object, e.g. a delicate biological tissue, can be largely avoided, yet the state of the photon *does* change. This curious phenomenon, namely one party affecting the other without a reciprocal action, was studied earlier on the basis of an underlying mechanism termed "quantum oblivion" [36]. That analysis turned out to underlie some other related phenomena too. Indeed, when a photon is employed in interaction-free measurement, its relative phase changes, but the "bomb" system, apparently oblivious to the interaction, does not change. It is this non-reciprocity that enables gathering information while minimizing induced disturbance.

## 5. Discussion

In summary, we have demonstrated a new imaging method termed Interaction-Free Ghost-Imaging (IFGI) and have shown how it can serve as a useful ghost-imaging technique to observe light sensitive structured objects. When compared with conventional ghost-imaging (CGI), a comparable SNR can be obtained with IFGI while reducing the number of photons illuminating the object up to 26.5%. Moreover, if one is to allow the same number of photons to illuminate that object as in CGI, IFGI is then capable of improving the SNR by 18%. The extra interferometer in the IFGI setup also makes the proposed technique sensitive to phase shifts and polarisation changes of light introduced by the observed object, whose effects are mostly invisible to CGI.

Optics EXPRESS

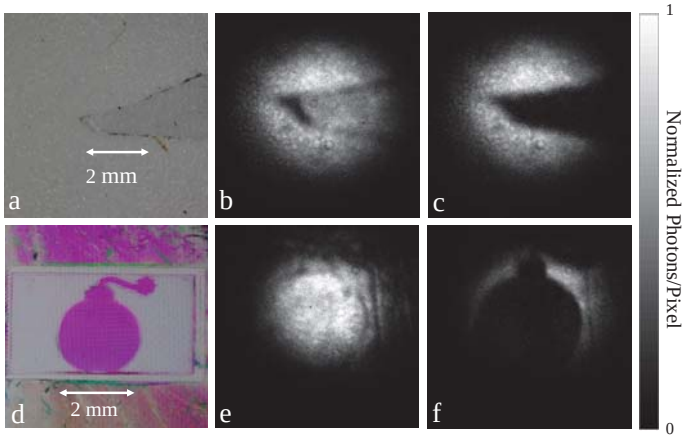


Fig. 6. Comparison between CGI and IFGI when imaging a phase-only and a birefringent object. A 0.15-mm-thick glass shard (a) is imaged with CGI (b) and IFGI (c). A polarization dependant "bomb" pattern imprinted on a liquid crystal device (d) imaged with CGI (e) and IFGI (f). The VBS is adjusted to 50:50 when taking the IFGI images and $t_{\text{int}} = 300$s for all images.

Thus IFGI would prove useful in imaging biological samples where changes in the sample thickness and composition can be observed. This sensitivity to phase and polarisation has also been demonstrated with ghost-imaging using classical light [39]. However, the "interaction-free" nature of this experiment is a purely quantum phenomenon and can be used to reduce the number of photons required to probe a light sensitive object which is otherwise not achievable with classical light. To realize the full potential of the IFGI technique, an ICCD camera that can be simultaneously triggered by two separate single photon detectors should be used. To our knowledge such a camera is currently not available on the market, but we believe modifying existing ICCD camera technologies to have this capability should not have any big technical difficulties. Potentially, one can further improve the capabilities of the IFGI technique by implementing the quantum Zeno effect [9, 10]. In light of the above demonstrative results, additional promising avenues are waiting to be explored, such as extending the technique to X-rays [40, 41], where reducing the amount of absorbed radiation by the tissues is vital.

## Appendix

### *Theoretical SNR of IFGI*

In Fig. 7(a), when an average of $\bar{N}$ photons enters a Mach-Zehnder interferometer with the input BS having reflectivity $R$ and transmissivity $T$, and the exit BS having reflectivity $T$ and transmissivity $R$, $\bar{N}$ photons will be detected in the constructive exit port and 0 photons detected in the destructive exit port. When an object is placed in one arm of the interferometer, as seen in Fig. 7(b), the single photon interference at the exit BS will be lost and we will have $\bar{N}R^2$ photons detected in the constructive port and $\bar{N}RT = \bar{N}R(1-R)$ photons detected in the destructive port. Now, in the constructive exit port, a change in photon number of $\Delta N_C = \bar{N}(R^2-1)$ with a variance of $\sigma^2(\Delta N_C) = \bar{N}(R^2+1)$ will be observed, and in the destructive exit port, a change of $\Delta N_D = \bar{N}RT = \bar{N}R(1-R)$ with variance $\sigma^2(\Delta N_D) = \bar{N}R(1-R)$ will be observed. Subtracting $\Delta N_D$ from $\Delta N_C$ gives,

$$\Delta N_{\text{IFGI}} = \Delta N_C - \Delta N_D = \bar{N}(2R^2 - R - 1), \tag{6}$$

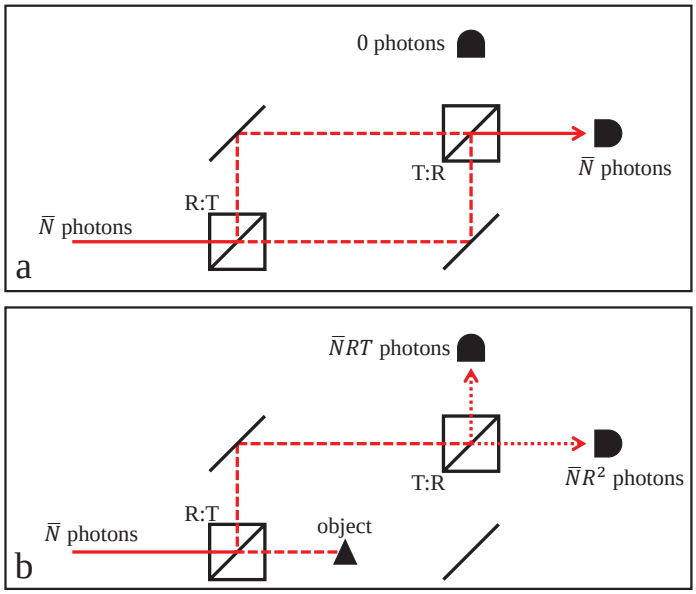


Fig. 7. Diagram depicting the average number of photons that will be detected at each detector in an interaction free measurement before (a) and after (b) an object is placed inside one arm of the interferometer.

with the variance given by,

$$\sigma^2(\Delta N_{\mathrm{IFGI}}) = \sigma^2(\Delta N_C) + \sigma^2(\Delta N_D) = \bar{N}(R+1). \tag{7}$$

Finally, the SNR is,

$$\mathrm{SNR}_{\mathrm{IFGI}} = \frac{|\Delta N_{\mathrm{IFGI}}|}{\sigma(\Delta N_{\mathrm{IFGI}})} = \frac{\left|2R^2 - R - 1\right|}{\sqrt{1+R}}\sqrt{\bar{N}}. \tag{8}$$

Here the average number of photons interacting with the object is $\bar{N}T = \bar{N}(R-1)$. If one were to allow $\bar{N}$ photons to interact with the object, then a total number of $\bar{N}' = \bar{N}/(R-1)$ photons must enter the interferometer and Eq. (8) becomes,

$$\mathrm{SNR}_{\mathrm{IFGI}} = \frac{\left|2R^2 - R - 1\right|}{\sqrt{1+R}}\sqrt{\bar{N}'} = \frac{\left|2R^2 - R - 1\right|}{\sqrt{1-R^2}}\sqrt{\bar{N}}. \tag{9}$$

### *Key specifications of equipment*

The Lumentum Xcyte CY-SM100 is a quasi-continuous wave laser with a power of 100 mW at 355 nm wavelength. The repetition rate is 100 MHz and the pulse duration is 10 ps.

The Excelitas SPCM-AQRH-14-FC SPAD has a maximum dark count rate of 100 counts/s and a quantum efficiency of close to 70% at 710 nm. However, due to poor coupling of the SPDC photons into the fibre and loses in the system due to imperfections in the optics and limited numerical aperture, the overall detection efficiency may be as low as 20% or less.

The Andor iStar CCD 334 is an intensified CCD camera that can be gated at 500 kHz by an external electric signal (here generated by our SPAD from detecting a photon). The photodiode in our camera is a 3rd generation model from Andor whose model number is 18x-73. The quantum efficiency of the photodiode at 710 nm is approximately 20%.

More details on the specifications of the equipments can be found on the manufacturer's websites at https://www.lumentum.com/, http://www.excelitas.com and https://andor.oxinst.com/.

Optics EXPRESS

### *Subtraction of background and accidental events*

The subtraction of background and accidental events in ghost imaging is shown in Fig. 8. First an raw image of the object, Fig. 8(a), is taken by setting the camera shutter to open in coincidence with the arrival of an entangled photon. Then the background and accidental events, Fig. 8(b), are taken by adjusting the camera delay such that the opening of the shutter is delayed by one laser pulse (10 ns for our laser, in the case of a CW laser, any timing delay greater than the gating time will work). The two images are then subtracted to obtain our final image, Fig. 8(c).

From Fig. 8(b), we see that there is a constant background of roughly 7860 counts/pixel which is from the electronic noise in the camera; there are some environmental background light seen in the bottom right corner of the image, and the bright circular region is mainly from accidental coincidences caused by statistical generation of multiple entangled photon pairs at the BiBO crystal. The total amount of background plus accidental coincidence events detected in Fig. 8(b), after the subtraction of the 7860 counts/pixel electronic noise, is approximately $4 \times 10^5$ counts/second, and that of real coincidence events from Fig. 8(c), is approximately $7.6 \times 10^5$ counts/second. If we focus only on the brightest region in Fig. 8(c) (region inside the "O"), we get approximately 12 coincidence events per pixel per second. From the same region in Fig. 8(b), there is an average of approximately 0.7 accidental coincidence events per pixel per second.

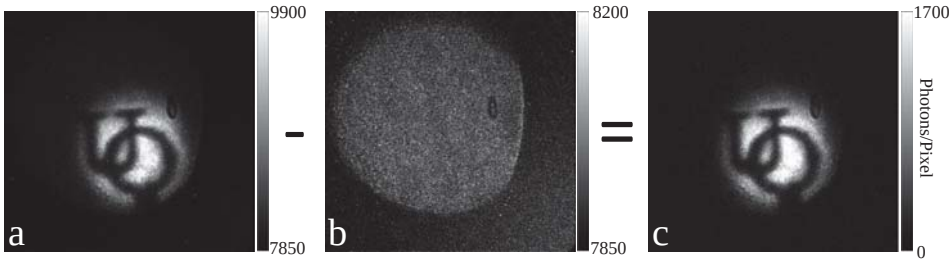


Fig. 8. Background subtraction in ghost imaging. Final image (c) is obtained by subtracting from the raw image (a), taken when the shutter of the camera is adjusted to coincide with the arrival of an entangled photon, from the background/accidental events (b), taken when the shutter is delayed by one laser pulse (10 ns) such that all coincidence events detected are due to the background/accidentals. Integration time is 150s.

### *IFGI images for different VBS ratios*

Figure 9 shows the images taken with IFGI with their corresponding SNR at various VBS R:T ratios. The images are all taken with the same integration time $t_{\text{int}} = 150$ s. Figure 10 shows the images taken for various VBS R:T ratios when the total number of interacting photons $N_{\text{int}}$ is the same in all cases. This is done by having $t_{\text{int}} = 150/(1 - R)$ s for each image.

Optics EXPRESS

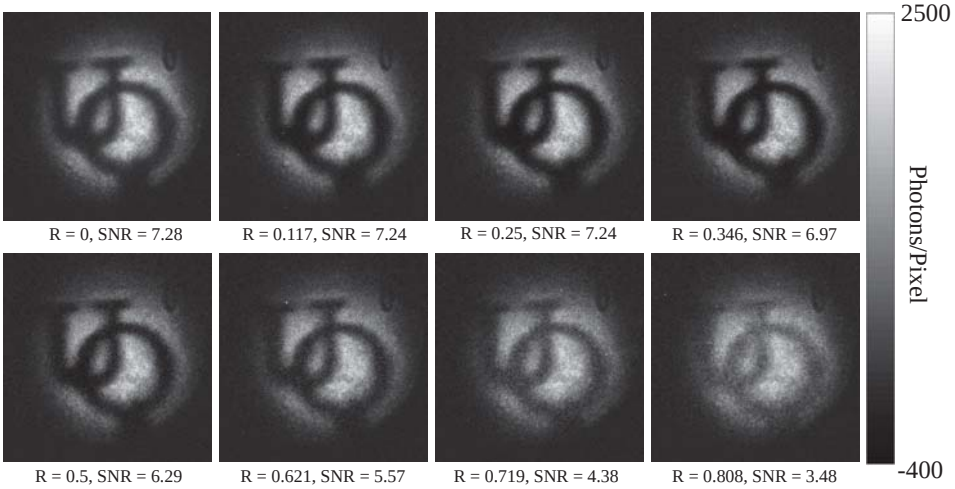


Fig. 9. Images taken with IFGI and their corresponding SNR at various VBS R:T ratios for $t_{\text{int}} = 150$ s.

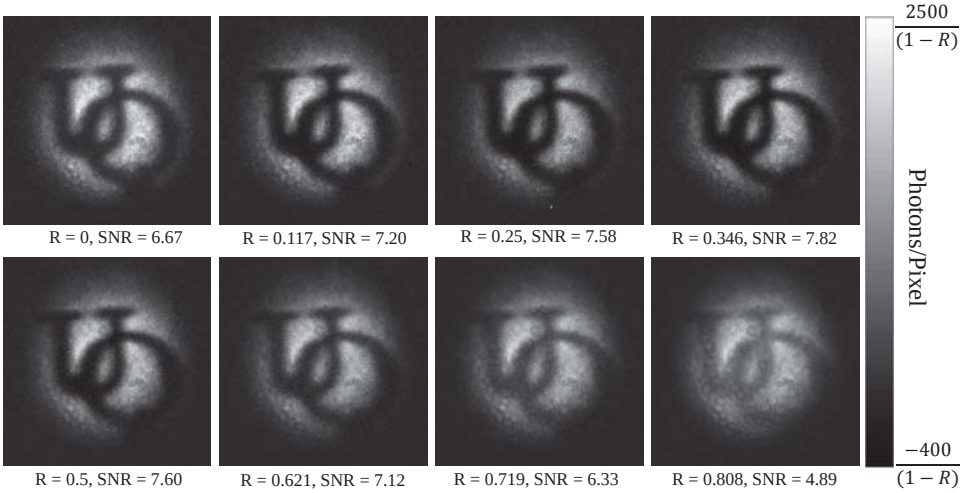


Fig. 10. Images taken with IFGI and their corresponding SNR at various VBS R:T ratios for $t_{\text{int}} = 150/(1-R)$ s allowing $N_{\text{int}}$ to be the same in all cases.

## Funding

Canada First Research Excellence Fund; Canada Research Chairs; Canada Foundation for Innovation; Canada Excellence Research Chairs.

## Acknowledgments

The authors acknowledge Robert Fickler, Peter Morris, Miles Padgett and John Sipe for helpful discussions

## References

1. V. Giovannetti, S. Lloyd, and L. Maccone, "Advances in quantum metrology," Nat. Photonics **5**, 222–229 (2011).
2. A. C. Elitzur and L. Vaidman, "Quantum mechanical interaction-free measurements," Foundations Phys. **23**, 987–997 (1993).
3. M. J. Padgett and R. W. Boyd, "An introduction to ghost imaging: quantum and classical," Philos. Trans. R. Soc. Lond. **375**, 20160233 (2017).
4. J. H. Shapiro and R. W. Boyd, "The physics of ghost imaging," Quantum Inf. Process. **11**, 949–993 (2012).
5. M. W. Mitchell, J. S. Lundeen, and A. M. Steinberg, "Super-resolving phase measurements with a multiphoton entangled state," Nature **429**, 161 (2004).
6. G. Brida, M. Genovese, and I. Ruo Berchera, "Experimental realization of sub-shot-noise quantum imaging," Nat. Photonics **4**, 227 (2010).
7. N. Samantaray, I. Ruo-Berchera, A. Meda, and M. Genovese, "Realization of the first sub-shot-noise wide field micscope," Light. Sci. & Appl. **6**, e17005 (2017).
8. A. G. White, J. R. Mitchell, O. Nairz, and P. G. Kwiat, ""interaction-free" imaging," Phys. Rev. A **58**, 605–613 (1998).
9. P. Kwiat, H. Weinfurter, T. Herzog, A. Zeilinger, and M. A. Kasevich, "Interaction-free measurement," Phys. Rev. Lett. **74**, 4763–4766 (1995).
10. P. G. Kwiat, A. G. White, J. R. Mitchell, O. Nairz, G. Weihs, H. Weinfurter, and A. Zeilinger, "High-efficiency quantum interrogation measurements via the quantum zeno effect," Phys. Rev. Lett. **83**, 4725–4728 (1999).
11. G. B. Lemos, V. Borish, G. D. Cole, S. Ramelow, R. Lapkiewicz, and A. Zeilinger, "Quantum imaging with undetected photons," Nature **512**, 409–412 (2014).
12. O. Hosten, M. T. Rakher, J. T. Barreiro, N. A. Peters, and P. G. Kwiat, "Counterfactual quantum computation through quantum interrogationt," Nature **439**, 949–952 (2005).
13. Y. Cao, Y.-H. Li, Z. Cao, J. Yin, Y.-A. Chen, H.-L. Yin, T.-Y. Chen, X. Ma, C.-Z. Peng, and J.-W. Pan, "Direct counterfactual communication via quantum zeno effect," Proc. Natl. Acad. Sci. **114**, 4920–4924 (2017).
14. J. Peise, B. Lücke, L. Pezzé, F. Deuretzbacher, W. Ertmer, J. Arlt, A. Smerzi, L. Santos, and C. Klempt, "Interaction-free measurements by quantum zeno stabilization of ultracold atoms," Nat. Commun. **6**, 6811 (2015).
15. P. Bierdz and H. Deng, "A compact orbital angular momentum spectrometer using quantum zeno interrogation," Opt. Express **19**, 11615–11622 (2011).
16. K. T. McCusker, Y.-P. Huang, A. S. Kowligy, and P. Kumar, "Experimental demonstration of interaction-free all-optical switching via the quantum zeno effect," Phys. Rev. Lett. **110**, 240403 (2013).
17. A. V. Belinskii and D. N. Klyshko, "Two-photon optics: diffractlon, holography, and transformation of two-dimensional signals," JETP **78**, 259 (1994).
18. T. B. Pittman, Y. H. Shih, D. V. Strekalov, and A. V. Sergienko, "Optical imaging by means of two-photon quantum entanglement," Phys. Rev. A **52**, R3429–R3432 (1995).
19. R. S. Aspden, D. S. Tasca, R. W. Boyd, and M. J. Padgett, "Epr-based ghost imaging using a single-photon-sensitive camera," New J. Phys. **15**, 073032 (2013).
20. R. Meyers, K. S. Deacon, and Y. Shih, "Ghost-imaging experiment by measuring reflected photons," Phys. Rev. A **77**, 041801 (2008).
21. P. A. Morris, R. S. Aspden, J. E. C. Bell, R. W. Boyd, and M. J. Padgett, "Imaging with a small number of photons," Nat. Commun. **6**, 5913 (2015).
22. R. S. Aspden, N. R. Gemmell, P. A. Morris, D. S. Tasca, L. Mertens, M. G. Tanner, R. A. Kirkwood, A. Ruggeri, A. Tosi, R. W. Boyd *et al.*, "Photon-sparse microscopy: visible light imaging using infrared illumination," Optica **2**, 1049–1052 (2015).
23. R. S. Bennink, S. J. Bentley, and R. W. Boyd, ""two-photon" coincidence imaging with a classical source," Phys. Rev. Lett. **89**, 113601 (2002).
24. F. Ferri, D. Magatti, A. Gatti, M. Bache, E. Brambilla, and L. A. Lugiato, "High-resolution ghost image and ghost diffraction experiments with thermal light," Phys. Rev. Lett. **94**, 183602 (2005).
25. R. S. Bennink, S. J. Bentley, R. W. Boyd, and J. C. Howell, "Quantum and classical coincidence imaging," Phys. Rev. Lett. **92**, 033601 (2004).
26. D. Duan, S. Du, and Y. Xia, "Multiwavelength ghost imaging," Phys. Rev. A **88**, 053842 (2013).
27. Y. Bai and S. Han, "Ghost imaging with thermal light by third-order correlation," Phys. Rev. A **76**, 043828 (2007).

Optics EXPRESS


28. Y. Cai and S.-Y. Zhu, "Ghost imaging with incoherent and partially coherent light radiation," Phys. Rev. E **71**, 056607 (2005).
29. G. Brida, M. V. Chekhova, G. A. Fornaro, M. Genovese, E. D. Lopaeva, and I. R. Berchera, "Systematic analysis of signal-to-noise ratio in bipartite ghost imaging with classical and quantum light," Phys. Rev. A **83**, 063807 (2011).
30. M. N. O'Sullivan, K. W. C. Chan, and R. W. Boyd, "Comparison of the signal-to-noise characteristics of quantum versus thermal ghost imaging," Phys. Rev. A **82**, 053803 (2010).
31. M. Genovese, "Real applications of quantum imaging," J. Opt. **18**, 073002 (2016).
32. H. Larocque, J. Gagnon-Bischoff, F. Bouchard, R. Fickler, J. Upham, R. W. Boyd, and E. Karimi, "Arbitrary optical wavefront shaping via spin-to-orbit coupling," J. Opt. **18**, 124002 (2016).
33. B. Jack, J. Leach, J. Romero, S. Franke-Arnold, M. Ritsch-Marte, S. M. Barnett, and M. J. Padgett, "Holographic ghost imaging and the violation of a bell inequality," Phys. Rev. Lett. **103**, 083602 (2009).
34. M. D'Angelo, A. Valencia, M. H. Rubin, and Y. Shih, "Resolution of quantum and classical ghost imaging," Phys. Rev. A **72**, 013810 (2005).
35. A. C. Elitzur and S. Dolev, "Nonlocal effects of partial measurements and quantum erasure," Phys. Rev. A **63**, 062109 (2001).
36. A. C. Elitzur and E. Cohen, "Quantum oblivion: A master key for many quantum riddles," Int. J. Quantum Inf. **12**, 1560024 (2014).
37. C. Robens, W. Alt, C. Emary, D. Meschede, and A. Alberti, "Atomic "bomb testing": the elitzur–vaidman experiment violates the leggett–garg inequality," Appl. Phys. B **123**, 12 (2016).
38. L. Hardy, "Nonlocality of a single photon revisited," Phys. Rev. Lett. **73**, 2279–2283 (1994).
39. D.-J. Zhang, Q. Tang, T.-F. Wu, H.-C. Qiu, D.-Q. Xu, H.-G. Li, H.-B. Wang, J. Xiong, and K. Wang, "Lensless ghost imaging of a phase object with pseudo-thermal light," Appl. Phys. Lett. **104**, 121113 (2014).
40. A. Schori and S. Shwartz, "X-ray ghost imaging with a laboratory source," Opt. Express **25**, 14822–14828 (2017).
41. Y. Y. Kim, L. Gelisio, G. Mercurio, S. Dziarzhytski, M. Beye, L. Bocklage, A. Classen, C. David, O. Y. Gorobtsov, R. Khubbutdinov, S. Lazarev, N. Mukharamova, Y. N. Obukhov, B. Roesner, K. Schlage, I. A. Zalushnyy, G. Brenner, R. Roehlsberger, J. von Zanthier, W. Wurth, and I. A. Vartanyants, "Ghost imaging at an xuv free-electron laser," arXiv p. 1811.06855 (2018).